Glass Struct. Eng. (2023) 8:81–98
https://doi.org/10.1007/s40940-022-00180-2

RESEARCH PAPER

Performance of cable-supported glass façades under time-depending wind action

Fabio Rizzo · Chiara Bedon

Received: 29 December 2021 / Accepted: 30 April 2022 / Published online: 25 May 2022
© The Author(s) 2022

Abstract Cable supported glass façades are sensitive to wind action because of their flexibility. Conventional laboratory testing to check a façade reliability under the wind action is generally carried out by uniformly air pressure tests. However, the typical wind action on a surface is known to be not uniform because it varies due to building aerodynamics and wind flow turbulence, and this aspect should be properly considered for testing protocols. This paper discusses the structural response of cable-supported glass façades, through time history finite element (FE) analyses, under different wind action combinations that varies based on the building aerodynamics (plan shapes and roof curvatures), the wind direction (0° and 90°), and the glass panel position (up and down). Such a finding is further enforced by the presence of flexible supports for the constituent glass modules. The presented results show a strong dependence of the structural response on the wind action configuration, and thus suggest the need of new testing protocols for similar systems.

F. Rizzo
Department of Civil Engineering, Cracow University of Technology, Warszawska 24, 31-155, Krakow, Poland
e-mail: fabio.rizzo@universityresearch.it

C. Bedon (✉)
Department of Engineering and Architecture, University of Trieste, Via Valerio 6, 34127 Trieste, Italy
e-mail: chiara.bedon@dia.units.it

Keywords Glass façades · Building aerodynamic · Cable-supported glass façade · Wind tunnel test · Numerical modelling

1 Introduction

The increasingly use of glass for load-bearing applications in buildings and infrastructures proved to represent an open issue for structural designers (Bedon et al. 2018). On one side, novel boundary and restraint applications make the use of glass in buildings extremely versatile, compared to other constructional materials. On the other, several safety issues are still related to tensile brittleness and typical size effects for building applications, under various loading conditions.

Among others, wind effects for façade systems are responsible of stress and deflection peaks that should be properly limited, and even minimized, depending on the mechanical and geometrical features of the system object of study (Bedon et al. 2018). In most of cases, glazing windows and façades represent a highly fragile and vulnerable component for buildings, given that they are expected to act as physical barrier under a multitude of design actions. For this reason, several studies have been spent for the analysis, assessment and even optimization of several solutions of practical interest for design, such as façades in tall buildings (Ding and Kareem 2020) which are most sensitive to wind pressures. Design criteria for façades under wind actions have been elaborated and discussed in Simiu

and Hendrickson (1987), Overend et al. (2007), Brewer and Sammarco (2018). The potential and feasibility of fragility curves in support of efficient and conservative design of glass façades under wind pressure has been addressed in Lima-Castillo et al. (2019). Complex mechanical systems in which glass panels are braced by cable systems have been investigated in Yu et al. (2017). A smart control system for cable supported façades under wind or even blast has been proposed in Santos et al. (2014, 2016), to prevent extreme stress peaks in glass components under dynamic events.

The wind induced displacements were estimated by Rizzo et al. (2021) based on a numerical model calibrated towards full-scale laboratory experiments. It was observed that the wind action estimated by wind tunnel tests affects the façade structural response closely differently than laboratory air pressure tests commonly used to check the façade reliability. Results discussed by Rizzo et al. (2021) proved that the wind-structure interaction in the field of the glass façades should be investigated carefully to avoid air infiltration and undesired torsion in the supporting frame members. In the present paper, the attention is still focused on façade glass panels under wind pressure. Compared to literature studies, however, major efforts are spent on the characterization and analysis of wind effects based on original experimental pressure data. Further, the analysis is focused on a special typology of cable-supported façade systems. More in detail, the case-study curtain wall explored in Amadio and Bedon 2012a, b, c) is take into account and adapted to the present investigation. Based on efficient but refined finite element (FE) models developed in ABAQUS (ABAQUS computer software), a set of twelve non-linear dynamic analyses is carried out with the support of twelve time histories of wind pressure. Typical wind effects and façade behaviours are thus assessed from parametric analyses. Based on simple preliminary calculations, the effects of boundaries for such complex mechanical systems are also analysed in terms of corresponding performance indicators for design.

The purpose of this paper is to discuss the wind-structure interaction for glass façades to alarm codifiers and sway the scientific community on such a sensitive issue. The thesis supported is that the static air pressure tests reproduced in laboratory to assess glass façade against wind pressure are not reliable because the wind action is a dynamic force, and its time-depending effect should not be neglected (Rizzo et al. 2021). For the present study, more in detail, the wind action is estimated by wind tunnel tests on buildings covered with a hyperbolic paraboloid roof. The building prototype represent a sport arena and it was supposed to have very large and tall glass façades on the perimeter. The pressure coefficients on the lateral surfaces are estimated in wind tunnel for different wind angles and for different plan shapes. A special care is then given to the comparative investigation of wind–structure interaction on zones close to the flow detachment edge and on zones that are far away from the edges.

The novelty of this paper consists of a discussion on the structural response of cable-supported glass façades under a dynamic action induced by the wind, and as far as the authors know, there are no comparable scientific publication on this issue.

To this aim, Sect. 2 summarizes the façade geometry and mechanical characteristics, with evidence of some basic preliminary considerations, while Sect. 3 discusses the reference wind tunnel experimental setup and the wind action calculations that are used for time-dependent non-linear analyses. Numerical simulations are thus presented in Sect. 4, while Sect. 5 discusses the main results.

2 Structural setup of the cable-supported glass façade

2.1 Façade system

In this paper, the analysis is focused on the cable-supported glass façade originally explored in Amadio and Bedon (2012a, b, c). The modular unit is $L = 9$ m tall and composed of $B = 1.55$ m laminated glass sheets schematized in Figs. 1 and 2 ($H = 3$ m their maximum height). The glass layers are fully tempered, with a nominal characteristic tensile strength in bending up to 120 MPa (CNR 2013; EN 16612:2019). As also explained in Amadio and Bedon (2012a, b, c), to minimize the computational cost of simulations and simplify the analysis, the façade is assumed to be wide enough ($B \times n$ modules $\gg L$) to neglect the lateral restraints at the vertical edges of each module.

Moreover, it is assumed that each laminated glass panel has a total nominal thickness $t_{tot} = 24.52$ mm, as obtained by bonding two glass sheets ($t_1 = t_2 = 10$ mm) and a middle PVB-interlayer ($t_{PVB} = 4.56$ mm). The glass panels are braced by a system of steel vertical

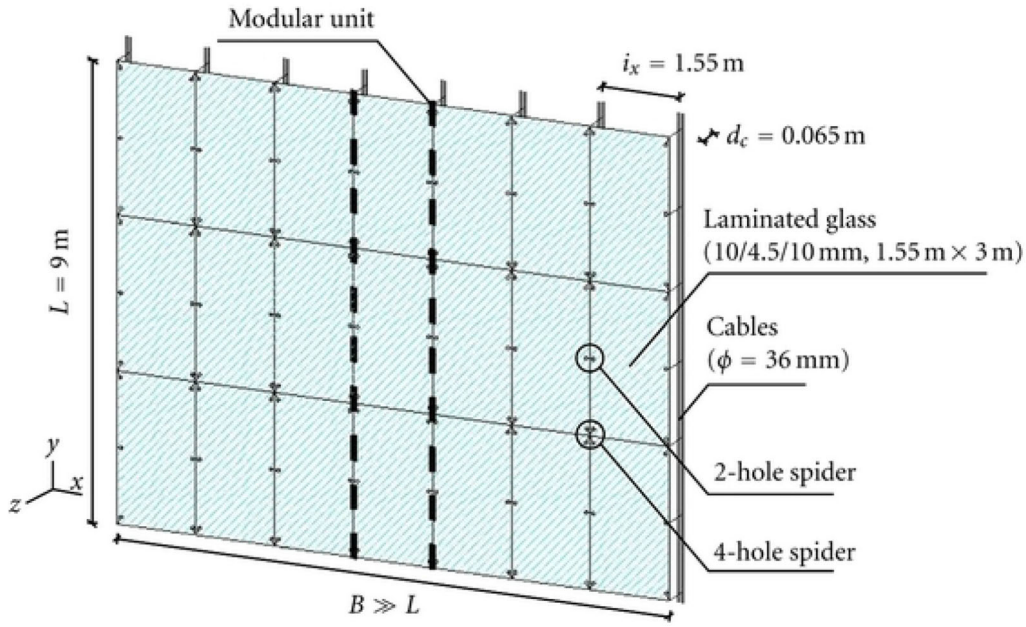

Fig. 1 Schematic drawing of the examined façade system, as adapted from (Amadio and Bedon 2012a, 2012b, 2012c). Figure reproduced from (Amadio and Bedon 2012c) under the terms and conditions of a Creative Commons Attribution License agreement

cables with $\phi = 36$ mm diameter. To realize an efficient bearing system for glass panels, they are spaced at intervals of $i_x = 1.55$ m in the plane of the wall (x-direction). At the same time, the distance between the bracing cables and laminated glass panels in z-direction is set equal to $d_c = 65$ mm.

A mostly rigid restraint in z-direction is offered by spider connectors with point-fixings (six point-fixings/glass panel) according to Fig. 2. The cable system is finally subjected to an initial prestressing force P_0.

2.2 Glass panel under quasi-static uniform pressure

The minimization of potential stress peaks and deflections in glass panels that are characterized by high slenderness and flexibility for curtain wall applications is—in most of cases—the primary target of design and analysis. Besides, boundary and restraint conditions are known to induce additional local and global behaviours that may result in premature fracture or exceedance of reference performance limit values.

For laminated glass panels under wind pressure, an equivalent quasi-static orthogonal pressure representative of wind action peak for the location of interest can provide useful preliminary feedback about the expected mechanical performance of the element. Stress and deflection peaks are thus verified against the prescribed limit values (CNR 2013; EN 16612:2019).

In the present paper, a preliminary comparative analysis for the $B \times L$ façade panel is presented in Fig. 3. At first, the viscous behaviour of interlayer is disregarded, and the analysis is carried out under the assumption of a "fully monolithic" glass section as in Fig. 3a, with $t_{tot} = 24.52$ mm. The quasi-static wind pressure W is uniformly applied to the full surface of glass. Two different boundary conditions are taken into account, namely the CS(A) configuration in Fig. 3b characterized by the presence of linear simple supports along the edges of glass and the "6PF(N)" configuration in Fig. 3c, where the glass panel is assumed restrained by six ideally rigid point-fixings. The corresponding stress and deflection peaks are monitored with the support of non-linear calculations as a function of the imposed pressure W.

Simple non-linear analytical calculations from CNR (2013); EN 16612:2019) are preliminary taken into account for the CS(A) configuration in Fig. 3b. This means that maximum stress values and deformations are estimated (both at the centre of glass panel) as:

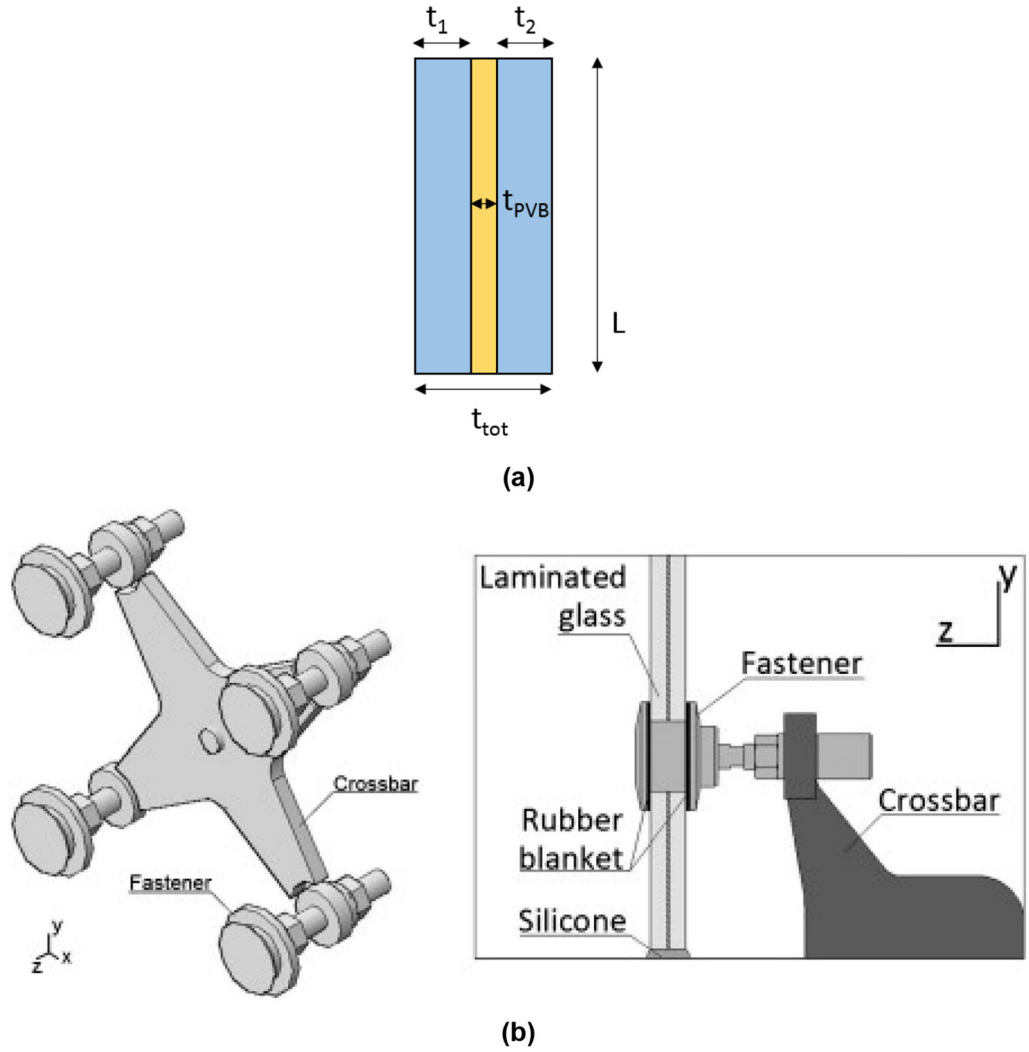

Fig. 2 Schematic drawing of façade details: **a** laminated glass section, **b** point-fixing connection

$$\sigma_{max} = k_1 \cdot \frac{A}{h^2} \cdot F_d \tag{1}$$

and

$$w_{max} = k_4 \cdot \frac{A^2}{h^3} \cdot \frac{F_d}{E} \tag{2}$$

In Eqs. (1) and (2), $A = B \times L$ is the surface of glass, F_d the design action corresponding to W, $h = t_{\text{tot}}$ the reference thickness, $E = 70$ GPa the Young's modulus of glass and k_1, k_4 two non-dimensional parameters (CNR 2013; EN 16612:2019). For the 6PF(N) configuration in Fig. 3c, the support of a simple FE numerical model is taken into account, due to the lack of efficient analytical formulations for such a specific restraint condition. The typical bending behaviour can be noted in Fig. 4a. Worth to remind that the stress and deflection peaks for the CS(A) case are expected at the centre of glass. Similar effects can be expected for the deflection analysis of the 6PF(N) panel with ideally rigid point-fixings, while stress peaks migrate from the panel centre towards the region of supports. In this regard, the numerical stress peaks calculated in the region of point-fixings need to be further magnified as in CNR (2013), that is:

$$\sigma_{hole} = \sigma \cdot K \tag{3}$$

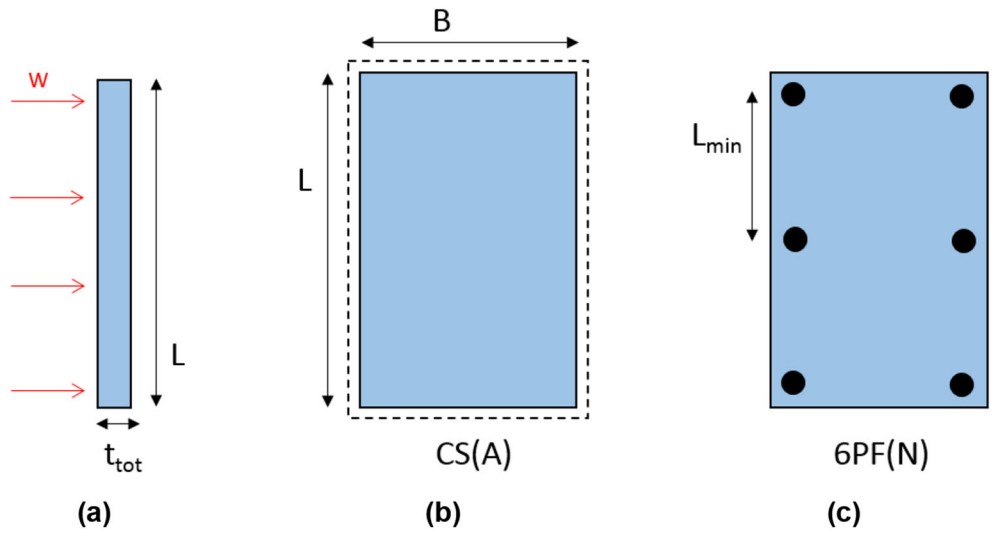

Fig. 3 Preliminary analysis of the glass panel under ideal boundary conditions and quasi-static wind pressure: **a** reference cross-section, **b** simple supported panel, **c** point-fixed panel

so as to account for the stress intensification factor K as in Fig. 4b, with $K \approx 2.1$ for the present calculation example. In this regard, it is important to remind that the modelling strategy according to Eq. (3) represents a practical but simplified approach, because the calculation is focused on the global effect induced by load distribution.

Comparative results are proposed in Fig. 4c for both the examined conditions, as a function of a uniform pressure W in the range of 0–30 kPa. The final effect of ideally rigid point-fixings is a stress peak increase denoted in Fig. 4c as "6PF(N) x K", which largely exceeds the stress estimates for the CS(A) condition.

As far as the actual restraint configuration of glass as a part of the cable-supported façade is disregarded, some additional feedback about the expected performance of the examined panel can be obtained by introducing in Fig. 4d the stress and deformation ratios. Ideal restraints, for a given panel shape, size and thickness, result in different performance limits for ultimate (stress) and serviceability (deflection) states. Following (CNR 2013), the maximum deflection in service conditions is limited to $H/60$ (or 50 mm) for the CS(A) panel. This deflection limit reduces to $L_{\min}/100$ (or 30 mm) for the 6PF(N) condition. Comparative plots exceeding the $y = 1$ value in Fig. 4d are thus representative of "unsafe" deformation amplitudes to avoid for design and serviceability checks. Worth to be noted in Fig. 4d, finally, is the trend of stress peaks towards the reference tensile resistance of glass.

Besides, all the comparative results in Fig. 4 still disregard the complex behaviour of the examined glass panel as a part of the cable-supported system in Figs. 1 and 2 (i.e., viscous behaviour of interlayer for the laminated section, flexibility of bracing cables, etc.), as well as the typical time variability and dependence of wind actions, thus recommending a detailed time-dependent analysis as in Sects. 3 and 4.

3 Wind action

The time-dependent wind action $W(t)$ on the examined façade was estimated according to Eq. (4), assuming the mean wind velocity V_m equal to 24.7 m/s; it was calculated assuming $v_{b00} = 31$ m/s, $z_0 = 0.7$, $z_{min} = 12$ m, $k_r = 0.23$, $a_0 = 500$ m, $k_a = 0.32$, the air density, $\rho = 1.25$ kg/m^3, A_i is the façades area (CEN (Comité Européen de Normalization) 2005). In Eq. (4) (CEN (Comité Européen de Normalization) 2005; CNR 2018), the time dependent pressure coefficients, $cp(t)$,were assumed according to results given by Rizzo et al. (2011) on lateral surfaces of building covered with large span roofs.

$$W(t) = cp_m(t) \cdot \left(\frac{1}{2}\rho {V_m}^2\right) \cdot A_i \tag{4}$$

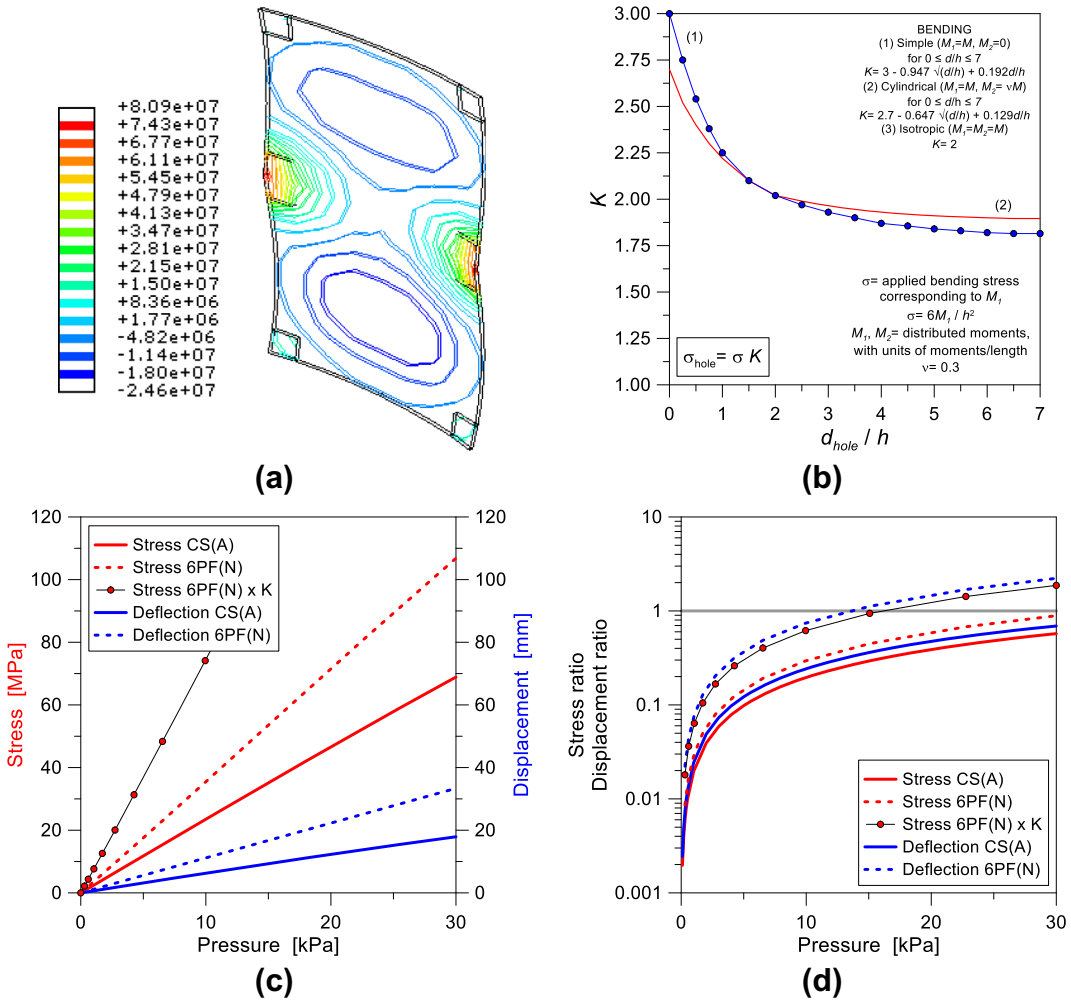

Fig. 4 Preliminary analysis of the glass panel under ideal boundary conditions and quasi-static wind pressure: **a** numerical model for 6PF(N), with legend values in Pa (shape scale factor × 5), **b** stress magnification factor K_t for bending, **c** stress–deflection trends and **d** stress–deflection ratios as a function of the imposed pressure (ABAQUS)

In total, eight different geometries of building were considered to investigate the influence of the building aerodynamics on the façade structural response. Table 1 and Fig. 5 summarize the reference geometries. The geometrical scale of the test model was assumed equal to 1:50.

Wind tunnel tests were carried out on four square and four rectangular building pressure models, all featuring a hyperbolic paraboloid roof, in the CRIACIV boundary layer wind tunnel in Prato, Italy (Rizzo et al. 2011). The facility is an open circuit tunnel with a 2.30 m × 1.60 m test chamber. The rigid models are made of wood and the number of pressures taps on the lateral surface ranges from 58 (i.e., Geometry #1, #3, #5 and #7) to 98 (i.e., Geometry #6 and #8). Each test models were equipped with Teflon tubing that was calibrated such to obtain a flat frequency response up to 100 Hz; this was achieved by selecting the tube length and the position of a pneumatic damper. Acquisition was carried out at a sampling frequency of 252 Hz for a duration of 29.7 s. The turbulence intensity at the roof level ranges between 11 and 12%. The tests were performed at a mean wind speed of 16.7 m/s at a height of 10 cm. Sixteen wind angles were acquired in wind tunnel but for sake of brevity results on only 0° and 90° (Fig. 5) are discussed in this paper.

Table 1 Geometrical properties of prototypes and test models

Geometry	L_1	L_2	f_1	f_2	H_1	$H_1 + f_1 + f_2$
Model (cm)						
#1	80.00	80.00	2.70	5.30	13.30	21.30
#2	80.00	80.00	2.70	5.30	26.70	34.70
#3	80.00	80.00	4.40	8.90	13.30	26.70
#4	80.00	80.00	4.40	8.90	26.70	40.00
#5	40.00	80.00	2.70	5.30	13.30	21.30
#6	40.00	80.00	2.70	5.30	26.70	34.70
#7	40.00	80.00	4.40	8.90	13.30	26.70
#8	40.00	80.00	4.40	8.90	26.70	40.00
Prototype (m)						
#1	40.00	40.00	1.35	2.65	6.65	10.65
#2	40.00	40.00	1.35	2.65	13.35	17.35
#3	40.00	40.00	2.20	4.45	6.65	13.35
#4	40.00	40.00	2.20	4.45	13.35	20.00
#5	20.00	40.00	1.35	2.65	6.65	10.65
#6	20.00	40.00	1.35	2.65	13.35	17.35
#7	20.00	40.00	2.20	4.45	6.65	13.35
#8	20.00	40.00	2.20	4.45	13.35	20.00

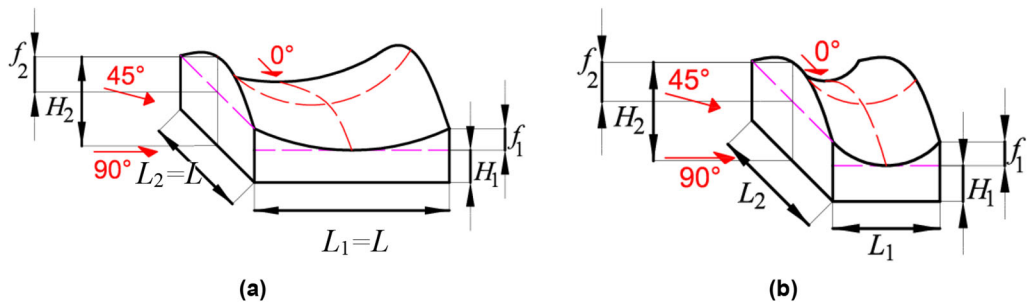

Fig. 5 Building geometrical parameters and wind angles of attack during experiments: **a** square plan and **b** rectangular plan building

The mean, maximum and minimum values of the pressure coefficients were calculated from the measured time series. In particular, the maximum and minimum values were calculated according to a best fit with the Gumbel distribution, following the procedure proposed by Cook and Mayne (1979) associated with a 22% probability of being exceeded, as it is done by Cook and Mayne (1979).

Buildings were covered with a double curvature roof (i.e., hyperbolic paraboloid roof) to simulate a cable net tensile structure. It was made of downward cables parallel to the 0° wind direction and upward cables parallel to 90° wind direction. The building lateral surfaces were divided in subzones as it is represented in Fig. 6 from 1 to 7 for square plan building and from 1 to 5 on the side parallel to 90° and from 1 to 7 on the side parallel to 0° (Fig. 6). Sides are named α, β, χ and γ clockwise. It was investigated because the flow field around the building lateral surfaces is very different on zones close to the detachment edges, as for example zones #1 and #7, and on zones very distant to the detachment edges as for example zone #4. However, it is necessary to distinguish two parts in the same zones, the part close to the upper edge and the part close to the floor. The flow field is different for these two parts of the façade and consequently it is loaded differently.

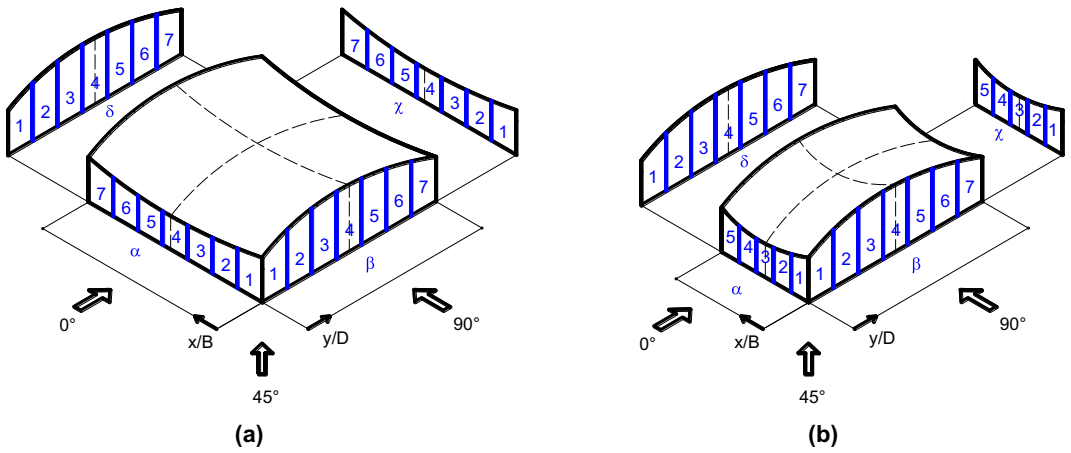

Fig. 6 Building lateral surface subzones: **a** square plan and **b** rectangular plan building

The different flow field and consequently the different wind action along the same façade affects the façade reliability because it can induce torsional effects on the façade beams and pillars. It can induce the detachment of the sealing gasket and consequently the air infiltration inside the building with a negative pressure from inside to outside.

In order to investigate this effect, four different sets of action listed in Table 2 were considered for this study (in the following, Combination #1, #2, #3 and #4). Each set consisted of two analyses for set #1, two analyses for set #2, four analyses for set #3 and four analyses for set #4, that have the purpose to compare the façade structural response under different environmental conditions. The exact definition of each set is discussed in the following. For sake of brevity, moreover, only selected geometries from Table 1 are discussed in this paper, and specifically geometries #1, #2, #3, #4 and #6. Load combinations was selected to highlight the differences induced by the building geometry and the wind flow trend.

It is in fact important to specify that the full set of geometries are named geometry #1 to #8 as in Table 1. There, the subzones are representative of the façade zones illustrated in Fig. 6, where they are labelled from #1 to #7 for all four sides of square plan building, or from #1 to #5 and from #1 to #7 for shorter and longer sides respectively of rectangular building.

The first set (i.e., Combination #1) consists of two analyses with the aim to investigate the influence of the aerodynamic due to the flow streamlines from the detachment zone; the second set (i.e., Combination #2) consists of two analyses with the aim to study the influence of the wind angle (i.e., 0° and 90°); the third combination (i.e., Combination #3) consists of four analyses with the aim to investigate the influence of roof

Table 2 Numerical analyses sets

Combination	Analysis	
#1	(I)	Wind action in subzone 1, geometry #4 [Ref. Table 1], side β, 0°
	(II)	Wind action in subzone 4, geometry #4 [Ref. Table 1], side β, 0°
#2	(I)	Wind action in subzone 1, geometry #3 [Ref. Table 1], side β, 0°
	(II)	Wind action in subzone 1, geometry #3 [Ref. Table 1], side β, 90°
#3	(I)	Wind action in subzone 2, geometry #1 [Ref. Table 1], side β, 0°
	(II)	Wind action in subzone 2, geometry #3 [Ref. Table 1], side β, 0°
	(III)	Wind action in subzone 2, geometry #1 [Ref. Table 1], side β, 90°
	(IV)	Wind action in subzone 2, geometry #3 [Ref. Table 1], side β, 90°
#4	(I)	Wind action in subzone 1, geometry #2 [Ref. Table 1], side β, 0°
	(II)	Wind action in subzone 1, geometry #6 [Ref. Table 1], side β, 0°
	(III)	Wind action in subzone 1, geometry #2 [Ref. Table 1], side β, 90°
	(IV)	Wind action in subzone 1, geometry #6 [Ref. Table 1], side β, 90°

curvature; finally, the fourth combination (i.e., Combination #4) consists of four analyses with the aim to investigate the influence of the building plan geometry (i.e., square and rectangular) for the two wind angle investigated.

Specifically, Combination #1 investigates, through two time-history analyses, the difference of the façade response induced by the distance from the detachment edge with wind angle equal to 0°. It has been done using wind tunnel experimental data elaborated for the geometry #4 (Table 1), the wind angle (0°) on the same side β, for two subzones, #1, close to the detachment edge, and #4, distant from the detachment edge.

Combination #2 investigates, through two time-history analyses, the difference of the façade response induced by a different wind angle. To achieve this purpose, the wind tunnel experimental data on geometry #3 under two different wind angle, 0° and 90°, on the same side β, for the subzones, #1, close to the detachment edge.

Combination #3 investigates, through four time-history analyses, for the same subzone quite close to the detachment edge (i.e. subzone #2), the difference induced by two wind angles (0° and 90°) and the difference induced by a different roof curvature, flat (i.e. geometry #1) and curved (i.e. geometry #3).

Finally, Combination #4 investigates, through four time-history analyses, for the same subzone close to the detachment edge (i.e. subzone #1), the difference induced by two wind angles (0° and 90°) and the difference induced by a different plan shape, square (i.e. geometry #2) and rectangular (i.e. geometry #6).

The selected combinations shall reflect any geometrical combinations available from experimental data. All calculations were computed using a wind action time history with a time length equal to 800 s and a time step equal to 0.1 s. For all analyses two-time histories were applied on the glass panel, the first one 1/4 of the glass panel height from the border down and the second one 1/4 of the glass panel height from the border up.

4 Structural time history analyses

4.1 Reference model

The parametric numerical analysis of the cable-supported glass system under wind pressure was carried out in ABAQUS (ABAQUS computer software). To this aim, the reference numerical model was derived from Amadio and Bedon (2012a, b, c) and adapted to the examined loading conditions. Composite shell elements (S4R) were used to describe the glass panels, while beam (B31) and truss (T3D2) elements realized the spider connectors and bracing system of cables, respectively. The final assembly consisted of 3900 DOFs and around 600 elements (Fig, 7a).

Linear elastic constitutive laws were used for materials. For fully tempered glass, the Young's modulus, Poisson' ratio and density were set in $E_g = 70$GPa, $\nu_g = 0.23$ and $\rho_g = 2500$ kg/m^3. Furthermore, for the PVB-interlayer, an equivalent elastic–plastic characteristic curve was taken into account, with $E_{PVB} = 8$ MPa the reference secant modulus corresponding to short-term wind actions (CNR 2013), with $\nu_{PVB} = 0.49$ and $\rho_{PVB} = 1100$ kg/m^3. Finally, harmonic steel (cables) and stainless steel (joints) were assumed to have a linear elastic behaviour, with $\rho_s = 7800$ kg/m^3, $\nu_s = 0.3$ and $E_{s,h} = 130$ GPa, $E_{s,s} = 170$ GPa respectively.

Based on the above material assumptions, especially for glass, the analysis of possible damage mechanisms (i.e., stress peaks in the region of point-fixings) were based on the time-dependent analysis of maximum stress and deformations for the full model components.

A special role was assigned to restraints, for the façade module assessment. The cables were pinned at the upper end, while the initial pretension force P_0 for the bracing system was imposed at their base in the form of an equivalent vertical displacement (see also Sect. 5.2). Along the elevation of the façade-module, only z-displacements and x-rotations were allowed for the other cables nodes, so as to account for the presence of adjacent façade members. Structural silicone sealant bonding glass panes was neglected, since it provides a negligible rotational stiffness (Amadio and Bedon 2012a, b, c). Each half-spider connector consisted in three rigidly connected 2-node linear beams that were linked by means of a weld connector (null relative displacements and rotations) and additional joins (pinned connectors with free relative rotations) to provide the

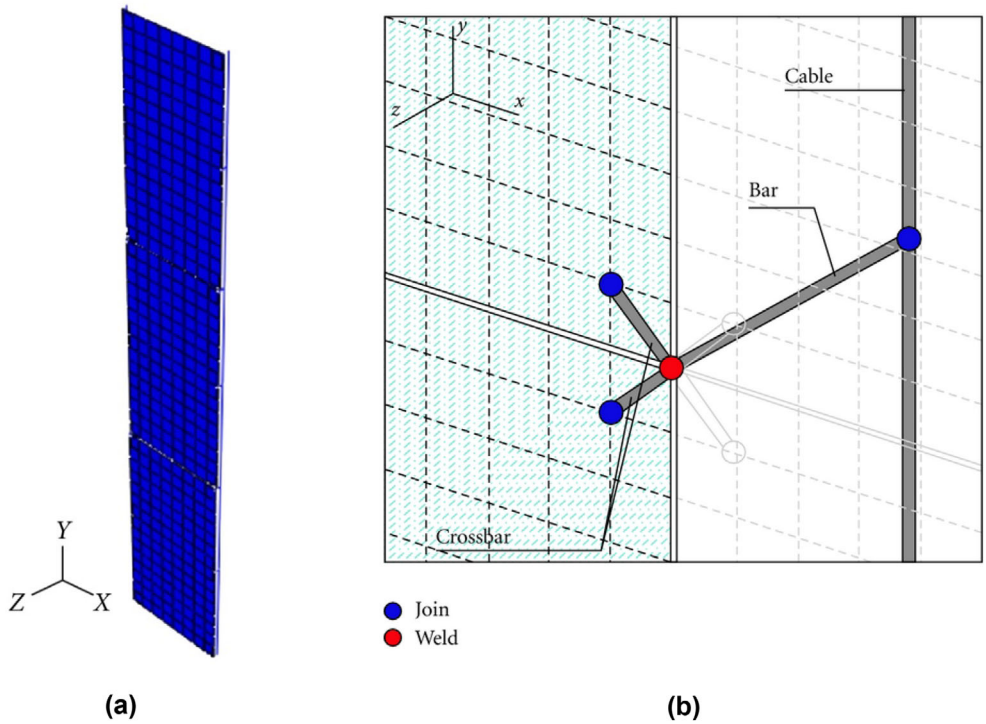

Fig. 7 Model of the façade module (ABAQUS): **a** general view and **b** schematic drawing of point-fixings. Figures reproduced from (Amadio and Bedon 2012c) under the terms and conditions of a Creative Commons Attribution License agreement

mechanical interaction of glass-spider and spider-cable nodes. A schematic drawing is proposed in Fig. 7b.

4.2 Analysis procedure and performance indicators

The typical analysis was arranged onto two steps. First, the façade system was subjected to self-weight and prestress force P_0 in the bracing cables (static step). Secondly, the preloaded model was analysed under the effects of wind pressures as in Table 2 (dynamic step). This step consisted of 60,000 increments over the duration of wind action.

For the post-processing stage, careful attention was paid for the analysis of some key indicators for the performance assessment of the façade module under wind actions. These included possible tensile stress peaks in glass (region of point-fixings, centre of panels); maximum out-of-plane deflections (centre of panels); relative deformation and twist of glass panels; as well as maximum stress peaks in the bracing cables. A dynamic approach through time history analyses is considered in the present study, because of its intrinsic advantages for nonlinear cables structures. A schematic view of reference control points and parameters is shown in Fig. 8.

For the analysis of wind effects on such a structural system characterized by flexibility parameters (and thus stress–deflection performance indicators) highly sensitive to the features of the bracing system of cables, some preliminary comparative calculations were carried out for the façade module.

The analysis was focused on the effects of initial prestress P_0 on the expected fundamental vibration period of the façade module (linear modal step), as well as on the maximum effects due to a quasi-static uniform wind pressure (non-linear static step). To this aim, the characteristic axial resistance of bracing cables is also recalled, with $P_{Rk} = 1150$ kN (Amadio and Bedon 2012a, b, c), so as to express the prestressing levels of bracers as a function of the imposed force towards the resistance.

As it can be seen in Fig. 9a, no marked variations can be expected in the qualitative fundamental vibration shape of the façade module under limited prestress

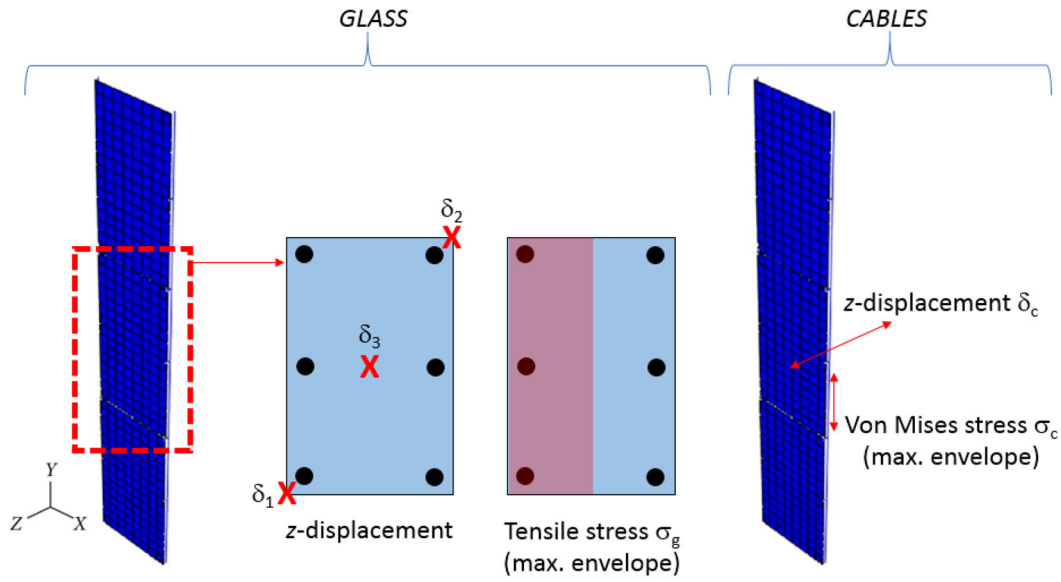

Fig. 8 Key performance indicators for the dynamic analysis of the façade module

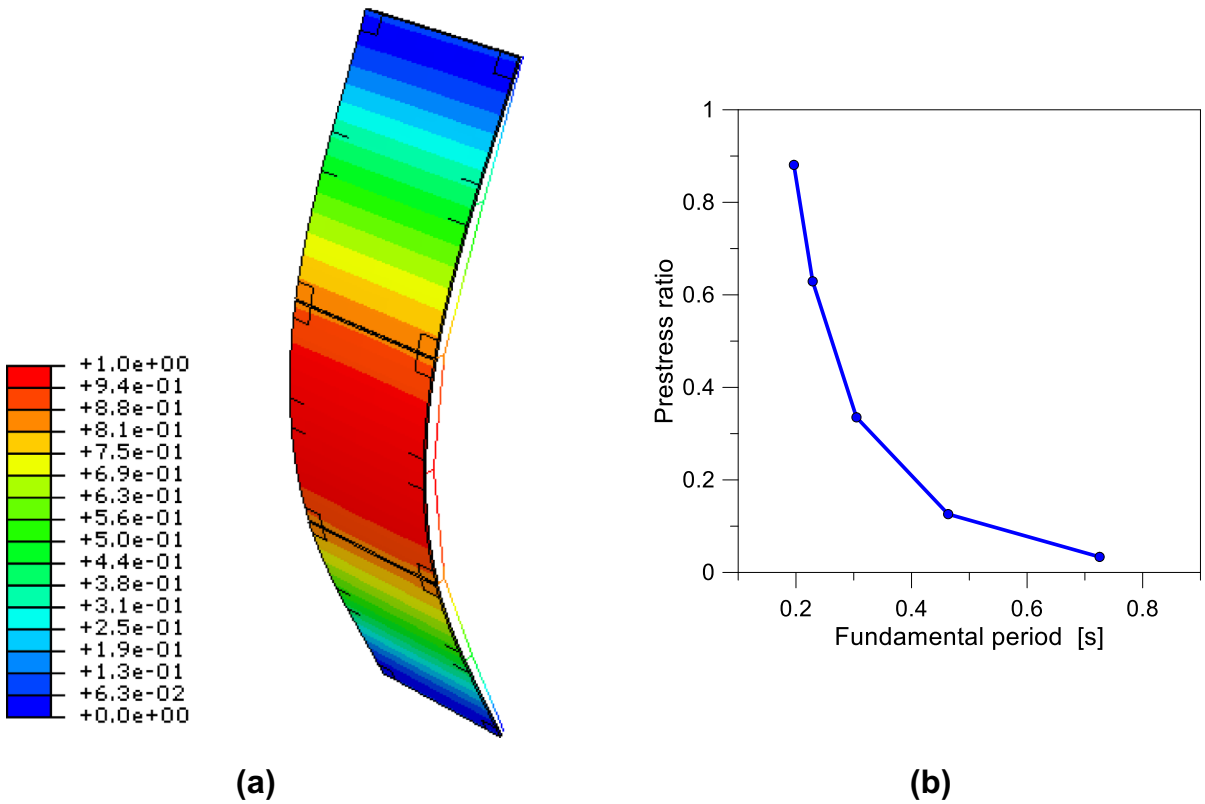

Fig. 9 Analysis of pretension effects in terms of **a** fundamental vibration shape and **b** period (ABAQUS)

ratio levels. Besides, marked modifications of the corresponding vibration period are recorded in Fig. 9b from the same parametric modal analyses.

A more detailed analysis of results for the deflection and stress performance of the central glass panel subjected to major bending effects can be summarized as in Fig. 10. There, the relative and absolute deflection ratios are first explored, due to the high flexibility of the system. Figure 10a shows the ratio of relative deflection (i.e., left-down minus middle central point of the panel) towards the allowable limit deflection reported in Sect. 2 (i.e., $L_{min}/60 = 15$ mm as in Fig. 4). The chart data in Fig. 10a that exceed the $y = 1$ value, in this regard, represent unsafe pressure amplitudes. Another important parameter for the dynamic performance analysis is the absolute deflection of the 9.00 m tall façade. To this aim, the global deflection under ordinary wind pressure should be limited to a maximum of 1/100 the total span (Amadio and Bedon 2012a, b, c). In this regard, chart data in Fig. 10b which exceed the $y = 0.001$ value are representative of unsafe pressure amplitudes for wind. In both figures, it is wort to mention that the effect of prestress level (even under quasi-static pressure assumptions) still reflects in marked modification of the façade performance.

In this regard, Fig. 10c shows the typical distribution of maximum principal stresses for the central laminated glass panel (10 kPa the pressure amplitude). It can be notice that the expected stress peaks in glass—thanks to the flexibility of supports—are relatively low, compared to the reference material resistance and to the corresponding deflection parameters. Most importantly, the deformed shape of the panel (and thus the corresponding stress distribution in glass) strongly differs from the idealized analysis of the plate with rigid point-fixings as in Fig. 4, thus confirming the importance of refined calculations for design purposes.

5 Discussion of time-dependent dynamic results

The parametric analysis with time-dependent wind pressure was carried out for the façade module characterized by a moderate prestress level in the cables, corresponding to $T_1 = 0.465$ s of fundamental vibration period as in Sect. 4. The quantitative analysis of parametric data was again carried out based on the performance indicators and selected control points previously discussed.

In Fig. 11, qualitative results are proposed for selected façade components and input pressure data.

As expected from the preliminary calculation steps, the façade module was characterized by limited stress peaks in glass, thus ensuring a mostly elastic response of the system under the imposed time histories. This can be noticed from the example of contour plots as in Fig. 11. The deformed shape of the system, even still characterized by a cylindrical deformation in accordance with the fundamental modal shape in Fig. 9, was also found to suggest local and global effects due to the non-uniform, time-dependent pressure histories for wind.

In this regard, Fig. 12 shows a quantitative overview of the structural response given by FE Analysis #1. Specifically, Fig. 12a presents the left-down corner displacement (δ_1) time history, Fig. 12b the right-up corner (δ_2) displacement time history, Fig. 12c the middle point displacement (δ_3) time history respectively. Figure 12d also shows the cable displacement (δ_c), while the corresponding envelope of Von Mises cable stresses (σ_c) is proposed in Fig. 12e. Worth to be noted the evolution of stress peaks in the glass panel (σ_g in Fig. 12f.

The collected stress peaks, as shown, are relatively small to avoid any kind of damage in the façade module components, or maximum deflections exceeding the reference limit values. Besides, the attention from the parametric numerical analysis outcomes is focused in the present study on the range of variability for the estimated performance indicators, as a major effect due to the time-dependency of wind pressures.

The statistics of output data are summarized in Tables 3 and 4 for all Combinations (i.e., from #1 to #4) and corresponding FE analyses (based on Table 2). Table 3 gives the mean, maximum, minimum and standard deviation value for displacements δ_1, δ_2 and δ_3. At the control points in the central glass panel. Similarly, Table 4 summarizes the variation of cable deflection δ_c and the maximum (envelope) stress parameters for cables (σ_c) and glass (σ_g).

For Combination #1 in Table 3, the comparison between subzone #1 (i.e., Analysis I) and subzone #4 (i.e., Analysis II) shows a very large difference for the selected control points (i.e., left-down, right-up and the middle one) especially observing the mean value that is opposite. This means that subzone #1 is in suction and subzone #4 is in pressure. This cannot be neglected

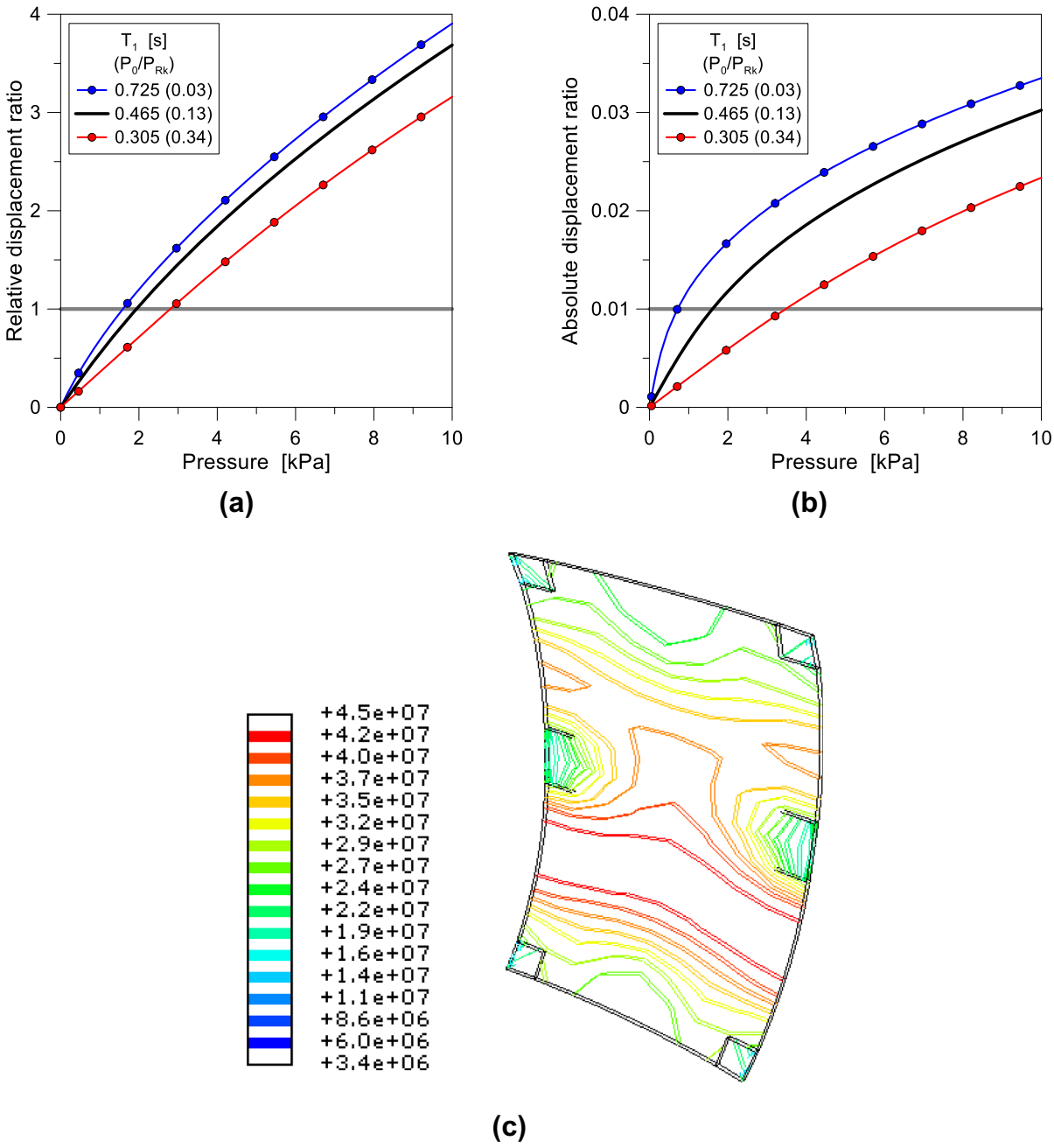

Fig. 10 Analysis of pretension effects in terms of **a**–**b** deflection and **c** stress analysis of the central glass panel under quasi-static uniform wind pressure (ABAQUS, shape scale factor × 5)

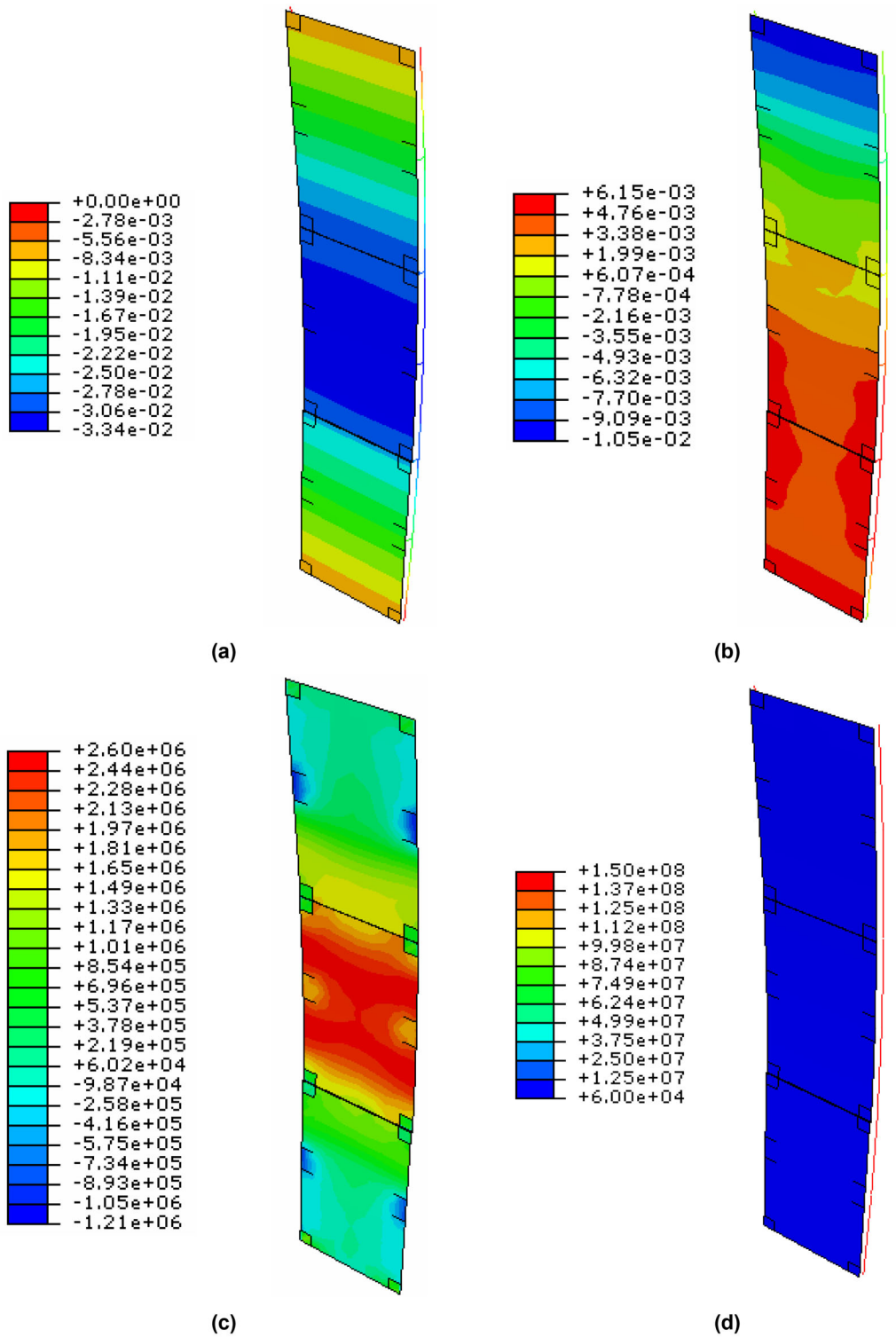

Fig. 11 Example of variation in time of: **a** deflection (in m), **b** velocity (in m/s), **c** maximum stress in glass (in Pa) and **d** Von Mises stress in cables (in Pa). ABAQUS/Standard, results from combo #3(ii) after 0.25 s of wind exposure

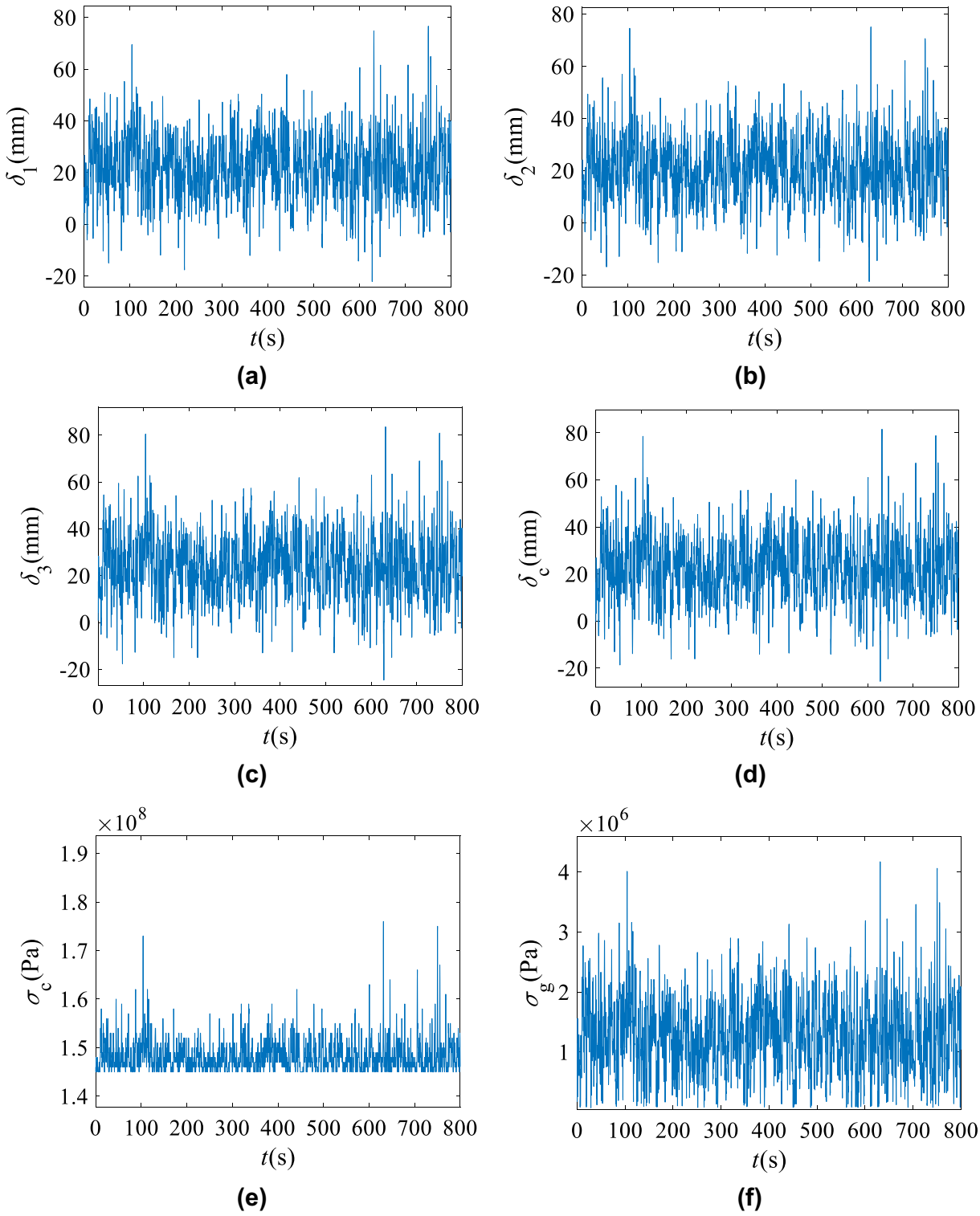

Fig. 12 Glass panel response for Analysis #1: **a** left-down corner displacement (δ_1), **b** right-up corner displacement (δ_2), **c** middle point displacement (δ_3), **d** cable displacement (δ_c), **e** cable Von Mises stress (σ_c) and **e** maximum principal stress in the glass panel (σ_g)

Table 3 Maximum (M), minimum (m), mean (μ) and standard deviation (σ) of the glass panel displacements, as measured at the left-down corner (δ_1), right-up corner (δ_2), or middle point (δ_3)

Comb	Analysis #	δ_1 (up)				δ_2 (middle)				δ_3 (down)			
		μ (mm)	M (mm)	m (mm)	σ(mm)	μ (mm)	M (mm)	m (mm)	σ(mm)	μ (mm)	M (mm)	m (mm)	σ(mm)
#1	(I)	20.41	75.06	− 22.52	12.12	23.71	83.54	− 24.59	13.16	22.19	76.66	− 22.11	11.85
	(II)	− 19.33	4.97	− 47.55	8.60	− 20.63	3.32	− 48.99	8.41	− 18.16	0.46	− 40.78	6.55
#2	(I)	4.05	54.20	− 51.80	15.51	5.30	58.93	− 56.48	16.23	5.30	51.44	− 50.24	13.83
	(II)	64.95	111.59	1.49	10.43	68.81	123.66	0.82	11.73	58.29	106.89	− 0.38	10.78
#3	(I)	12.77	64.14	− 32.57	14.60	14.21	69.49	− 36.30	15.22	12.59	58.23	− 33.18	13.00
	(II)	4.05	54.20	− 51.80	15.51	5.30	58.93	− 56.48	16.23	5.30	51.44	− 50.24	13.83
	(III)	67.80	113.81	1.49	10.40	71.60	114.39	0.82	11.31	60.40	98.10	− 0.38	10.18
	(IV)	64.95	111.59	1.49	10.43	68.81	123.66	0.82	11.73	58.29	106.89	− 0.38	10.78
#4	(I)	38.38	57.63	1.49	5.68	40.96	69.21	0.82	7.48	35.07	67.10	− 0.38	8.08
	(II)	− 9.99	16.17	− 38.21	7.81	− 9.06	14.78	− 35.45	7.37	− 6.48	12.78	− 27.28	5.54
	(III)	38.10	79.11	1.49	6.89	41.23	89.30	0.82	6.52	35.89	78.18	− 0.38	4.94
	(IV)	74.68	103.45	1.49	5.74	74.96	113.90	0.82	6.33	59.08	97.50	− 0.38	5.88

during the design phase the façade. In Table 3, standard deviation was assumed as a measure of the time-depending effect of wind pressure. It can be observed that for combination #1 it ranges from 6.55 (right-up, subzone #4) to 13.16 (middle point, subzone #1). As it was expected the flow field is more instable close to the detachment edge (i.e., subzone #1) and that is the reason because the standard deviation is bigger on this subzone. However, this effect should be taken into account during the design phase because it means that the façade sealing gasket are more loaded by wind induced vibration in subzone #1 than in subzone #4.

For Combination #2, based on values given in Table 2, it was observed that due to the building shape and its aerodynamics, the same subzone #1 is loaded very differently under wind angle 0° and 90°.

The mean value ranges from 5.30 mm to 68.81 mm in the middle point of the façade. It means that several wind angles should be investigated in the design the façade.

Based on data given in Table 3 for Combination #3 and for the same subzone #2, it was observed that the roof curvature affects the façade displacements because the mean value ranges from 5.30 mm (i.e., analysis (II)) to 14.21 mm (i.e., analysis (I)) with a wind angle equal to 0° (middle control point). At the same time, the measured deflection spans from 68.81 mm (i.e., analysis (IV)) to 71.60 mm (i.e., analysis (III)) with a wind angle equal to 90°, for the same control point. It was also noted that the variation of the mean value of measured displacements in the middle point is smaller for 90° than 0° due to the building aerodynamics.

All calculations herein discussed showed alternative positive and negative displacements induced by pressure and suction on the façade system, as a direct effect of wind dynamics.

Finally, as expected, data in Table 3 show a significant difference between square plan building and rectangular plan building for both two wind angles and combinations object of study.

A major sensitivity and variation of parametric FE results was observed for the cable displacement (δ_c), cable stress (σ_c) and glass panel stress (σ_g), as it can be seen in Table 4. The location of the glass panel around the building lateral surface affects results as well as the building roof curvature, the wind angle and the plan shape. Results in term of glass panel stress show that the maximum peak ranges from 0.17 Pa to 4.17 MPa. This variation is very large and should be properly taken into account for the optimal design of glass thickness and point-fixing detailing.

Most importantly, such a stress–deflection sensitivity to the imposed time-dependent wind pressure affects the design of structural details, and consequently further affects the resulting natural vibration period of

Table 4 Maximum (M), minimum (m), mean (μ) and standard deviation (σ) of cable displacement (δ_c), cable Von Mises stress (σ_c) and principal stress in the glass panel (σ_g)

Comb	Analysis #	δ_c				σ_c				σ_g			
		μ (mm)	M (mm)	m (mm)	σ (mm)	μ (MPa)	M (MPa)	m (MPa)	σ (MPa)	μ (MPa)	M (MPa)	m (MPa)	σ (MPa)
#1	(I)	22.32	81.58	− 25.62	13.05	148.16	176.00	145.00	3.12	1.28	4.17	0.07	0.61
	(II)	− 21.69	2.10	− 49.81	8.35	147.39	157.00	145.00	1.82	0.88	2.22	0.09	0.39
#2	(I)	4.06	57.27	− 57.24	16.12	146.24	160.00	145.00	1.70	0.71	3.00	0.07	0.50
	(II)	67.07	121.14	− 0.38	11.60	166.45	209.00	145.00	7.50	3.43	6.78	0.17	0.58
#3	(I)	12.91	67.78	− 37.24	15.11	146.77	164.00	145.00	2.38	0.91	4.13	0.07	0.61
	(II)	4.06	57.27	− 57.24	16.12	146.24	160.00	145.00	1.70	0.71	3.00	0.07	0.50
	(III)	69.84	112.26	− 0.38	11.19	168.22	206.00	145.00	7.52	3.56	6.08	0.17	0.55
	(IV)	67.07	121.14	− 0.38	11.60	166.45	209.00	145.00	7.50	3.43	6.78	0.17	0.58
#4	(I)	39.46	67.33	− 0.38	7.40	152.37	167.00	145.00	2.74	2.09	3.64	0.17	0.37
	(II)	− 10.21	13.49	− 36.40	7.32	145.80	152.00	145.00	0.99	0.40	1.58	0.08	0.26
	(III)	39.73	87.30	− 0.38	6.47	152.40	177.00	145.00	2.46	2.10	5.31	0.17	0.32
	(IV)	73.24	111.50	− 0.38	6.27	170.74	198.00	145.00	4.23	3.71	6.34	0.17	0.31

the façade and its dynamic response, once the optimal parameters are detected. The wind induced effect estimated by FE analyses suggest that the wind action should be reproduced carefully during the preliminary test of façade systems, because it is reasonable to think that the estimated variation will be closely more significant for the case of façades on high-rise buildings (Rizzo et al. 2020).

6 Conclusions

The performance of a typical cable-supported glass façades under time-depending wind action estimated in wind tunnel was investigated through time history Finite Element (FE) numerical analysis. A special care was given to wind action description as well as to local and global performance parameters. As known, for practical applications, the use of conventional protocols for loading single glass panels with ideal boundary restraints is rather consolidated and generally conservative approach. Besides, especially for complex and wide glass facades under live loads such as wind actions, a balance of modelling simplicity and accuracy of estimates (even on the safe side for design) should be properly addressed.

The wind action was calculated from pressure coefficients estimated in wind tunnel on lateral surface of low-rise buildings covered with a hyperbolic paraboloid roof under two orthogonal wind directions (i.e. 0° and 90°). It was investigated the dependence of the structural response on the building aerodynamics given by the building plan shape and the roof curvature, on the wind direction and on the panel location on the façade. The façade structural response was explored for panels close to or distant from the detached zone, and close to or distant from ground. Totally, twelve different wind action combinations were also considered in this study and the structural response was discussed in terms of structural performance indicators.

For example, as far as a global structural model is taken into account for glass panels, it was observed that the structural response in term of glass displacements and cable stress peaks varies considerably with random wind action, compared to conventional loading protocols. In addition, it was estimated that some zones are expected in pressure and some zones in suction, for the same façade components. This finding gives a torsion of the façade as a whole, that should be carefully analysed during the design phase. Finally, the time history action shows that pressure and suction are time-depending, and it means that two areas of the same panel can be loaded by pressure or suction at the same time.

Even if the wind induced local pressures are under the limits for glass panels, the wind action induced cinematics on the façade structural system might be unsafe.

Results suggest that the pressure test on the façades carried out in laboratory to simulate the wind action are not representing the real behaviour because they should take into account the pressure and suction alternative given by the buildings aerodynamics and by the wind flow turbulence. This paper aims to recommend a glass panel testing standard procedure update to simulate consistently the wind action on the glass panels taking into account effects due to the turbulence and to the aerodynamics.

Funding Open access funding provided by Università degli Studi di Trieste within the CRUI-CARE Agreement.

Declarations

Conflict of interest The authors declare that they have no conflict of interest.

Open Access This article is licensed under a Creative Commons Attribution 4.0 International License, which permits use, sharing, adaptation, distribution and reproduction in any medium or format, as long as you give appropriate credit to the original author(s) and the source, provide a link to the Creative Commons licence, and indicate if changes were made. The images or other third party material in this article are included in the article's Creative Commons licence, unless indicated otherwise in a credit line to the material. If material is not included in the article's Creative Commons licence and your intended use is not permitted by statutory regulation or exceeds the permitted use, you will need to obtain permission directly from the copyright holder. To view a copy of this licence, visit http://creativecommons.org/licenses/by/4.0/.

References

ABAQUS computer software, v. 6-12-1. Simulia

Amadio, C., Bedon, C.: Elastoplastic dissipative devices for the mitigation of blast resisting cable-supported glazing façades. Eng. Struct. **39**, 103–115 (2012a)

Amadio, C., Bedon, C.: Viscoelastic spider connectors for the mitigation of cable-supported façades subjected to air blast loading. Eng. Struct. **42**, 190–200 (2012b)

Amadio, C., Bedon, C.: Dynamic response of cable-supported façades subjected to high-level air blast loads: numerical simulations and mitigation techniques. Model. Simul. Eng. (2012c). https://doi.org/10.1155/2012/863235

Bedon, C., Zhang, X., Santos, F., Honfi, D., Kozłowski, M., Arrigoni, M., Figuli, L., Lange, D.: Performance of structural glass facades under extreme loads—design methods, existing research, current issues and trends. Constr. Build. Mater. **163**, 921–937 (2018)

Brewer TR, Sammarco EL (2018). Optimizing glass design: the role of computational wind engineering & advanced numerical analysis. In: Proceedings of Challenging Glass 6 -Conference on Architectural and Structural Applications of Glass. Louter, Bos, Belis, Veer, Nijsse (Eds.), Delft University of Technology, May 2018. https://doi.org/10.7480/cgc.6.2174.

CEN (Comité Européen de Normalization), Eurocode 1: Actions on structures—Part 1–4: General actions—Wind actions, EN-1991-1-4 (2005)

CNR (National Research Council of Italy). Istruzioni per la Progettazione, l'Esecuzione ed il Controllo di Costruzioni con Elementi Strutturali di Vetro, [Guide for the Design, Construction and Control of Buildings with Structural Glass Elements]. CNR-DT 210/2013, (2013). Free download of English version at: https://www.cnr.it/en/node/3843

CNR (National Research Council of Italy) Guide for the Assessment of Wind Actions and Effects on Structures. CNR-DT 207/2018 (2018)

Cook, N.J., Mayne, J.R.: A novel working approach to the assessment of wind loads for equivalent static design. J. Wind Eng. Ind. Aerodyn. **4**, 149–164 (1979)

Ding, F., Kareem, A.: Tall buildings with dynamic facade under winds. Engineering **6**(12), 1443–1453 (2020)

EN 16612:2019. Glass in building—determination of the lateral load resistance of glass panes by calculation. CEN, Brussels

Lima-Castillo, I.F., Gómez-Martínez, R., Pozos-Estrada, A.: Methodology to develop fragility curves of glass façades under wind-induced pressure. Int. J. Civil Eng. **17**, 347–359 (2019)

Overend, M., Zammit, K., Hargreaves, D.: Applications of computational wind engineering in the design of glass façades. Proc. Glass Perform. Days **2007**, 444–448 (2007)

Rizzo, F., D'Asdia, P., Lazzari, M., Procino, L.: Wind action evaluation on tension roofs of hyperbolic paraboloid shape. Eng. Struct **33**(2), 445–461 (2011)

Rizzo, F., Ricciardelli, F., Maddaloni, G., Bonati, A., Occhiuzzi, A.: Experimental error analysis of dynamic properties for a reduced-scale high-rise building model and implications on full-scale behavior. J. Build. Eng. (2020). https://doi.org/10.1016/j.jobe.2019.101067

Rizzo, F., Franco, A., Bonati, A., Maddaloni, G., Caterino, N., Occhiuzzi, A.: Predictive analyses for aerodynamic investigation of curtain walls. Structures **29**, 1059–1077 (2021)

Santos, F., Gonçalves, P.F., Cismaşiu, C., Gamboa-Marrufo, M.: Smart glass facade subjected to wind loadings. Proc. Inst. Civil En. Struct. Build. **167**(12), 743–752 (2014)

Santos, F., Cismasiu, C., Bedon, C.: Smart glazed cable facade subjected to a blast loading. Proc. Inst. Civil En. Struct. Build. **169**(3), 223–232 (2016)

Simiu, E., Hendrickson, E.M.: Design criteria for glass cladding subjected to wind loads. J. Struct. Eng. (1987). https://doi.org/10.1061/(ASCE)0733-9445(1987)113:3(501)

Yu, Y., Liu, T., Zhang, Q., Yang, B.: Wind-induced response of an L-shaped cable support glass curtain wall. Shock Vibr. (2017). https://doi.org/10.1155/2017/4163045

Publisher's Note Springer Nature remains neutral with regard to jurisdictional claims in published maps and institutional affiliations.